Electrochimica Acta 278 (2018) 340–351

Contents lists available at ScienceDirect

Electrochimica Acta

journal homepage: www.elsevier.com/locate/electacta

The properties and performance of carbon produced through the electrochemical reduction of molten carbonate: A study based on step potential electrochemical spectroscopy

Matthew A. Hughes [a], Jessica A. Allen [b], Scott W. Donne [a, *]

[a] Discipline of Chemistry, University of Newcastle, Callaghan, NSW, 2308, Australia
[b] School of Engineering, Priority Research Centre for Frontier Energy Technologies and Utilisation, University of Newcastle, Callaghan, NSW 2308, Australia

ARTICLE INFO

Article history:
Received 15 January 2018
Received in revised form
18 April 2018
Accepted 4 May 2018
Available online 25 May 2018

Keywords:
Electrodeposited carbon
Electrochemical capacitors
Molten carbonate reduction
Step potential electrochemical spectroscopy
Cyclic voltammetry
Carbon characterisation

ABSTRACT

Carbons with BET specific surface areas of 500 $m^2 g^{-1}$ have been produced through the electrolytic reduction of molten Li_2CO_3-K_2CO_3-Na_2CO_3 at the eutectic composition (43.5:25:31.5 mol%) onto graphite at 600 °C and 0.30 A cm^{-2} under a 60 mL min^{-1} CO_2 gas flow. These carbons have been shown to consist largely of amorphous carbon with some spherical and flake-like conglomerates. Functionalised oxygen has been observed in synthesised carbons using FTIR and XPS. Synthesised carbons have been investigated in 3-electrode cells and analysed using cyclic voltammetry and step potential electrochemical spectroscopy (SPECS) at room temperature. Capacitances as high as 450 F g^{-1} have been observed at 0.0833 mV s^{-1} scan rates. The EDLC and pseudo-capacitive behaviour of produced carbons have been analysed and it has been found that the produced carbons behave hybrid capacitors with considerable pseudo-capacitive contributions. The performance of synthesised carbons has been compared to that of activated carbon derived through the chemical activation of carbon from the pyrolysis of coconut husks and to the reported capacitances of commercial activated carbons.

1. Introduction

Since the mid-eighteenth century humanity has shown an ever-increasing reliance on access to efficient, affordable energy to facilitate transport, lighting, warmth, and the comforts of modern life [1]. Of particular importance to the functioning of many of these comforts of modern life is the reliable storage and release of electrical energy. In past and recent times much of this energy demand has been supplied by petroleum based fuels [2]; however, the environmentally damaging and inherently limited nature of petroleum based fuels make it necessary for alternative methods of energy storage to be pursued [1,2]. As such, in recent decades, a considerable amount of effort has been put into the development of efficient energy storage devices, particularly batteries, fuel cells, and supercapacitors.

Supercapacitive materials tend to have high surface areas and are able to form thin dielectric layers which enhance electric energy storage [2]. As a result of this, supercapacitors exhibit capacitances much greater than those of normal electrolytic capacitors [2]. Due to the lack of permanent chemical and physical changes that supercapacitors experience upon charge and discharge, the devices show good cycle-life and high specific power, but relatively low specific energy [3,4]. The discharge times for supercapacitors are, however, considerably shorter than those of batteries and fuel cells [5]. As such supercapacitor applications are relatively limited in areas where long term, slow release, electrochemical energy storage is desirable, such as in the energy supplies for vehicles, portable computers, and mobile phones; however, they are invaluable in areas such as memory protection, back-up power supplies, and in other areas requiring rapid charge-discharge cycling [2]. In recent years, there has been significant research directed towards increasing the specific energy of supercapacitors while maintaining the high specific power of the materials [3].

Supercapacitors may be separated into three major categories, each giving us some information about the electrochemical behaviour of the material. Electrochemical double layer capacitors (EDLCs) are non-faradaic devices in which energy storage occurs electrostatically, via positive-negative charge separation at the electrode-electrolyte interface [2,6,7]. Due to the absence of

* Corresponding author.
E-mail address: scott.donne@newcastle.edu.au (S.W. Donne).

https://doi.org/10.1016/j.electacta.2018.05.045
0013-4686/

chemical changes during their operation, EDLCs exhibit long cycle lives with good cycle stability [2]. The main electrode materials used in the construction of EDLCs are carbon-based materials, and the preferred methods of increasing the capacitance of these materials tends to be through increasing the surface area and electrical conductivity of the material [7]. Compared to this, pseudocapacitors store charge through fast, reversible redox reactions at or close to the electrode-electrolyte interface [7]. Supercapacitors of this form often consist of metal oxides (such as RuO_2) or conductive polymers [2,7]. This form of supercapacitor tends to show increased energy densities compared to EDLCs, at the expense of reduced cycle life [2]. The third class of supercapacitors are those of a hybrid structure which shows characteristics of both EDLCs and pseudocapacitors [2].

A range of materials may be used in supercapacitor devices depending upon the desired properties of the final device. Common materials used in the construction of these devices include transitional metal oxides, metal nitrides, metal sulfides, metal carbides, and carbon-based materials [2,8]. Carbonaceous materials in particular have been investigated as a cheap and flexible material for use in supercapacitors. Activated carbons and carbon gels with capacitances between 50 and 130 F g^{-1} in aqueous media have been previously investigated [9–11], as have carbon nanotubes [10–14], nano and mesoporous carbons [15–17], templated carbon nanostructures [18], and carbide-derived carbons [10,19,20]. Recent research into chemically modified graphene has produced composites of polyaniline electropolymerised onto the surface of graphene, which show capacitances as high as 230 F g^{-1} in aqueous sulfuric acid [8]; however, these materials are relatively complex to synthesise. As such it is desirable that a simpler, less expensive method of producing carbons for use as supercapacitor electrode materials be found. Of the potential methods for producing these carbonaceous materials investigated in recent years, a promising method is the electro-reduction of molten carbonate salts [21]. This path of carbon synthesis is of particular interest as a medium temperature method of producing carbonaceous products with physical properties that depend heavily on the conditions of deposition [21–29]; however, at this time, relatively little is known about the electrochemical performance and charge-storage potential of these materials. This work investigates charge storage mechanisms in carbons produced in a molten Li_2CO_3-K_2CO_3-Na_2CO_3 (43.5:25:31.5 mol%, [22]) eutectic under a set of standard conditions, with a particular focus being placed upon identification of the relative contributions of EDLC and pseudocapacitive charge storage on the total capacitance of these carbons. This is achieved through electrochemical characterisation by step potential electrochemical spectroscopy (SPECS) in three electrode cells. SPECS is a versatile technique which has previously been used to characterise the influence of applied potential and state of charge on the kinetics of diffusion through manganese dioxide electrodes [30–33], and in differentiating faradaic and non-faradaic charge storage contributions in manganese dioxide electrodes [34]. More recently the technique has also been adapted and expanded for use in the characterisation of charge storage processes in carbons and other electrode materials, with focus being placed on rate performance and the development of a suitable model for use in the analysis of SPECS results [35,36]. Due to the versatility of the SPECS technique it was judged to be a good analysis technique for use in the separation of charge storage contributions.

2. Experimental

2.1. Carbon synthesis

Carbons were synthesised in three electrode cells (Fig. 1) containing a molten ternary Li_2CO_3-K_2CO_3-Na_2CO_3 electrolyte at the eutectic composition (43.5:25:31.5 mol%). The ternary carbonate eutectic was prepared in house from Li_2CO_3, K_2CO_3 and Na_2CO_3 (Sigma-Aldrich, >99%). Carbonate powders were initially dehydrated under atmospheric conditions at 100 °C for at least 24 h following which the powders were mixed together at the eutectic composition and ball-milled at 170 rpm in 10 forward and 10 reverse, 2 min cycles using a Fritsch Pulverisette 6 zirconia ball mill. Ternary eutectics were fused at 500 °C for 1 h under a 60 mL min^{-1} CO_2 flow and allowed to cool to room temperature prior to being reheated for carbon synthesis.

The mechanism of carbon reduction was examined by cyclic voltammetry prior to bulk carbon electrodeposition so as to confirm that carbon deposition was proceeding without unexpected impurities. Electrochemical experiments were controlled using a Pine Wavenow potentiostat.

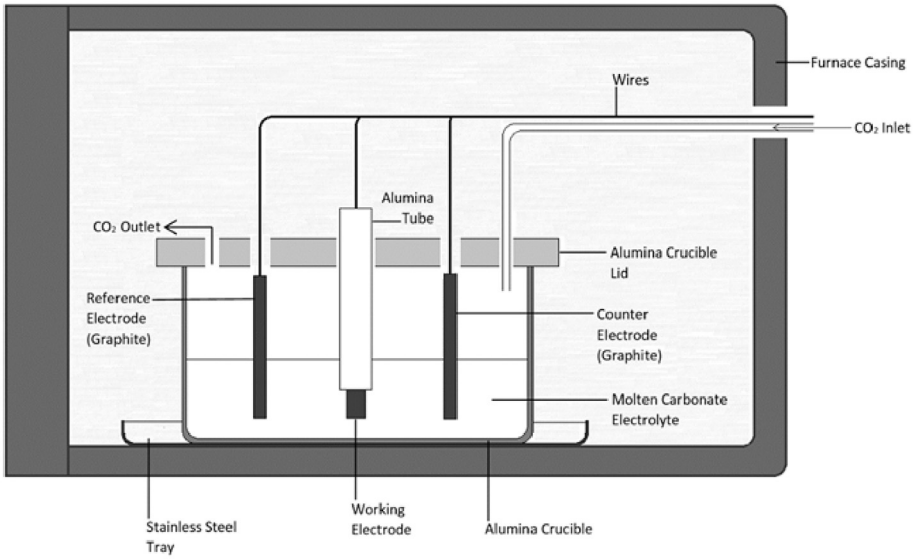

Fig. 1. Schematic for the electrochemical cell setup used throughout this research.

During carbon electrodeposition cells were heated to 600 °C (±1 °C) in a programmable LABEC ashing furnace at a rate of ~1.6 °C.min^{-1}. Carbon dioxide gas (BOC gases; food grade) was allowed to flow across the surface of the electrolyte at a rate of ~60 mL min^{-1}. The electrodes were held above the carbonate eutectic until it became molten, at which point they were submerged and allowed to equilibrate for 30 min prior to experimentation. Carbon electrodeposition was then carried out at a current density of 0.30 A cm^{-2} relative to the geometric surface area of the working electrode. The cell consisted of a cylindrical alumina crucible (Ceramic Oxide Fabricators) topped with an alumina lid which contained holes to allow for the placement of electrodes and a CO_2 inlet and outlet. Alumina forms a corrosion layer of lithium aluminate in the presence of molten carbonates, which increases the surface roughness of the material [37], but is otherwise stable under these harsh conditions, so was deemed suitable for use throughout this research. In all cases the pre-electrodeposition geometric surface area of the graphite working electrode exposed to the electrolyte (<1.0 cm^2) was considerably smaller than that of the graphite counter electrode (>7.0 cm^2). This minimised the influence of any reactions at the counter electrode on the deposition [38]. Following the electrodeposition process carbons were manually removed from the solidified carbonates and soaked in 1.0 M H_2SO_4 (prepared from 97% H_2SO_4, Sigma Aldrich) for at least 24 h to remove carbonate impurities.

2.2. Electrochemical characterisation

2.2.1. Electrode preparation

The capacitive performance of the carbon materials synthesised through the electrolytic reduction process were measured by forming the materials to be tested into inks, which were each used to construct the working electrode in a three-electrode cell. To create these inks, a mixture was prepared from 15 wt% synthesised carbon, 80 wt% Vulcan XC72R conductive carbon black (Cabot, 100%) and 5 wt% poly(vinylidene fluoride) (PVdF) binding agent (Sigma Aldrich, average $M_W \approx 534{,}000$ Da). This composition has previously been shown to be useful for the study of the electrochemical characteristics of materials in three-electrode cells [36]. This mixture of solid ingredients was ground lightly in a mortar and pestle to form a homogeneous powder. A small amount of this powder (~0.1 g) was taken and 3 mL of 1-methyl-2-pyrrolidinone (NMP; Sigma Aldrich; 99%) was added to form an ink. This ink was thoroughly mixed using a magnetic stirrer prior to use to promote homogeneity. This method was also used to prepare counter electrode ink from 80% activated carbon (prepared by previous groups through the pyrolysis and subsequent activation of coconut husks first at 500 °C under nitrogen, and then in concentrated H_3PO_4 at 700 °C under nitrogen [36]), 15% Vulcan XC72R conductive carbon black and 5% PVdF binding agent. This composition ensured that any limitations to the system were due to the working electrode.

Electrodes were prepared by pipetting 75 μL of the working electrode ink and 100 μL of the counter electrode ink onto the end of separate stainless steel substrates (d = 13 mm, l = 50 mm) using an Excalibur precision pipette. To promote binding the electrodes were well scrubbed with fine (1200 grit) emery paper and cleaned with acetone prior to the placement of inks. The ink was allowed to dry on the electrodes at 60 °C for at least 24 h, after which time a thin coating of electrode material remained on the end of each electrode.

2.2.2. Electrochemical cell preparation

The electrochemical cell was constructed using a Swagelok 13 mm perfluoro alkane (PFA) T-junction. The previously prepared electrodes were inserted into the ends of the T-junction with separator paper between them. The separator paper was soaked in 0.5 M H_2SO_4 prior to insertion in the cell. An electrolyte reservoir was prepared from a cut plastic pipette. The electrolyte reservoir was sealed to the top of the T-junction using parafilm. The electrodes were held in place with seals and screws-on covers. Once the cell was constructed, the electrodes were compressed at 250 psi for 5 min using a hydraulic press. The electrolyte reservoir was filled with 0.5 M H_2SO_4 and a saturated calomel reference electrode (Radiometer Analytical) was introduced. The area around the reference electrode was sealed using parafilm to prevent electrolyte evaporation during electrochemical testing.

2.3. Characterisation

2.3.1. Scanning electron microscopy (SEM)

A Zeiss Sigma VP FE-SEM fitted with a Bruker light element SSD EDS detector was used to examine the surface morphologies of the synthesised carbons. Finely ground carbon powders were lightly dusted onto sample holders covered with carbon paint. An accelerating voltage of 4 kV was used in most cases. Due to the conductive nature of the carbonaceous samples, gold or carbon coating was not required prior to SEM imaging.

2.3.2. Fourier transform infrared spectroscopy (FTIR)

Infrared spectra of carbon samples were recorded using a PerkinElmer UATR Two spectrophotometer. Spectra were collected over the interval 4000-400 cm^{-1} using 4 scans with a resolution of 2 cm^{-1}.

2.3.3. X-ray photoelectron spectroscopy (XPS)

XPS was performed on carbons using a Thermo ESCALAB250i X-ray photoelectron spectrophotometer in an ultra-high vacuum system (1×10^{-9} Pa) equipped with a hemispherical analyser. Carbon powders were rolled onto strips of indium foil (99.99%; thickness: 0.2 mm; CMR*direct*), obtaining a complete coating of carbon mounted on the metal surface. The indium strips were fixed to sample holders using double sided tape. The filled sample holders were degassed and transferred to the XPS analysis chamber. An unmonochromated Mg K_α X-ray source was used to supply an incident X-ray beam with energy 1253.7 eV. The spectrophotometer was calibrated based on the assumed binding energy (BE) of the Au4f$_{7/2}$ line (84.0 eV). The standard deviation for binding energy with this setup was given to be ±0.1 eV. Survey scans using a 1 eV step size were taken in the 0–600 eV range, following which detailed scans using a 0.25 eV step size were performed in the C 1s and O 1s regions. Data analysis was carried out using CasaXPS 2.3.16 software, with the background being approximated using the Shirley algorithm and spectra being fitted with Gaussian-Lorentzian functions.

2.3.4. Gas adsorption

The specific surface area of each carbon sample was determined from gas adsorption using a Micrometrics ASAP 2020 Surface Area and Porosity Analyser. Carbon samples (~0.02 g) were heated under vacuum at 300 °C for 24 h prior to analysis. Due to the high surface area and low mass of the sample this quantity of synthesized carbon was sufficient to determine the surface area of the material with minimal error from the sample size, with the literature indicating that, for carbons with surface areas comparable to those examined here, even 0.01 g can be sufficient to obtain a relatively accurate measure of BET specific surface area (SSA) [39]. A 9-point N_2 adsorption isotherm was taken at 77 K over the relative pressure range 0.05–0.30 P/P_O. This isotherm was used to determine the SSA of the examined carbon using the linearized BET isotherm.

2.3.5. Electrochemical characterisation

All electrochemical characterisation was carried out using an Iviumstat Multichannel Potentiostat controlled by Iviumstat software. The cell was allowed to equilibrate at open circuit potential (OCP) for 60 min, following which the potential was cycled for 250 cycles between −0.5 V and 0.3 V vs SCE at a rate of 25 mV s^{-1} to establish reversible cycling. Following this, step potential electrochemical spectroscopy (SPECS) was performed by stepping the potential from −0.5 V to 0.3 V vs SCE and back again with steps of ±0.025 V followed by 300 s equilibration periods. Analysis of the SPECS results was carried out in the R2017a build of MATLAB using non-linear least-squared error curve fitting based on the trust-region-reflective algorithm.

3. Results and discussion

3.1. Carbon deposition mechanism

The mechanism of carbon electrodeposition from molten carbonate salts was examined using cyclic voltammetry (CV) prior to the commencement of bulk electrodeposition (Fig. 2). Based on the lack of cathodic peaks present in Fig. 2, except for a gradual increase in current towards the cathodic limit corresponding to carbon electrodeposition, it can be concluded that carbon is electrodeposited in a process involving a single rate-determining step, based on the literature this may correspond to the 4-electron reduction mechanism; i.e. [19,22],

$$CO_3^{2-} + 4e^- \rightarrow C + 3O^{2-} \quad (1)$$

There are multiple anodic peaks apparent in Fig. 2. It is likely that these correspond to the oxidation of products formed during the reduction of molten carbonates by multiple processes. As only a single reduction process is observed, this likely corresponds to the oxidation of carbon phases by multiple paths, with possible processes including those shown in Fig. 2.

The presence of a cathodic hysteresis loop (~-1.75 V vs $C/CO_2/CO_3^{2-}$) in Fig. 2 is indicative that the carbon electrodeposited onto the graphite substrate is not identical to the electrode material. As amorphous carbon has a considerably greater electrical resistance than graphitised carbon (0.091 Ω cm compared to 0.029 Ω cm) [40] this may indicate that electrodeposited carbons do not consist solely of graphitised carbon, instead consisting, at least partly, of amorphous carbon with increased electrical resistivity. The deposition of carbon with increased surface areas onto the graphite substrate also contributes to the presence of this hysteresis loop. The lack of multiple reduction peaks in Fig. 2 is indicative that the major product of deposition is carbon, with lithium and lithium carbides being possible alternative products in the deposition potential region. These potential impurities would be removed effectively during post-deposition acid rinsing.

3.2. Morphology

High magnification SEM images were taken of carbons synthesised in the manner described above (Fig. 3). Carbons were observed to consist largely of amorphous phases with some spherical aggregates and plate-like structures being apparent. The presence of amorphous carbon is consistent with the conclusions presented previously based on mechanistic studies. The spherical aggregates and plate-like structures with well-defined end points were measured through comparison of the relevant dimensions to the scale of the image. This revealed that spherical aggregates in the synthesised carbons tended to be almost circular in profile, with both the average length and width of aggregates being close to 500 nm. The plate-like structures tended to show lengths of ~1900 nm, almost double the average width of 1000 nm. Some of the plates were also in an alignment such their thickness could be measured, hence we are able to estimate that the average thickness of the plate-like structures in the synthesised carbons is 50 nm. It is likely, based on the previous statement that carbon deposits onto graphite in a single electron transfer process that these different phases form at different times during the deposition process. Due to the different resistances and surface areas of the materials, the overpotential for graphitized phase formation on graphitized carbon should be slightly lower than the overpotential of amorphous phase formation on the material. In addition to this the initial surface area of the working electrode is slightly smaller that of it at later times during the deposition process, so the energy density of carbon deposition is higher. The combination of these factors may lead to the deposition of carbon in its more energetically stable graphitized state as an initial layer during carbon deposition, followed by the formation of an amorphous phase on top of this layer as the working electrode grows irregularly, which would lead to more dispersed, lower energy per unit area carbon deposition.

The bonding interactions in synthesised carbons were examined through the use of FTIR. Carbons tended to show spectra with few peaks, with the lack of peaks between 3700 and 3000 cm^{-1} or at

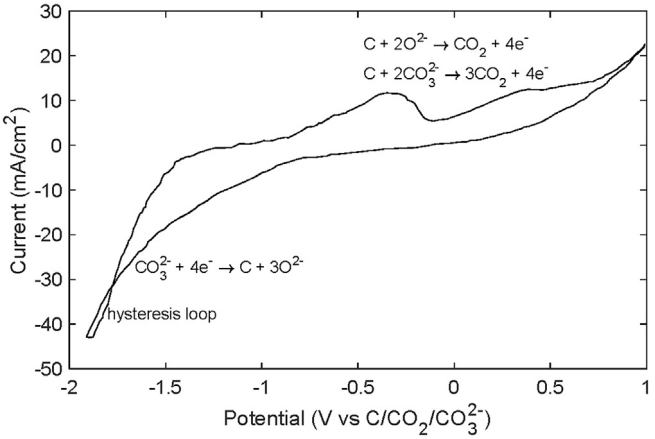

Fig. 2. The cyclic voltammogram for the electrolytic reduction of ternary Li_2CO_3-K_2CO_3-Na_2CO_3 eutectic at 600 °C using a graphite working electrode and a sweep rate of 5 mV s^{-1}.

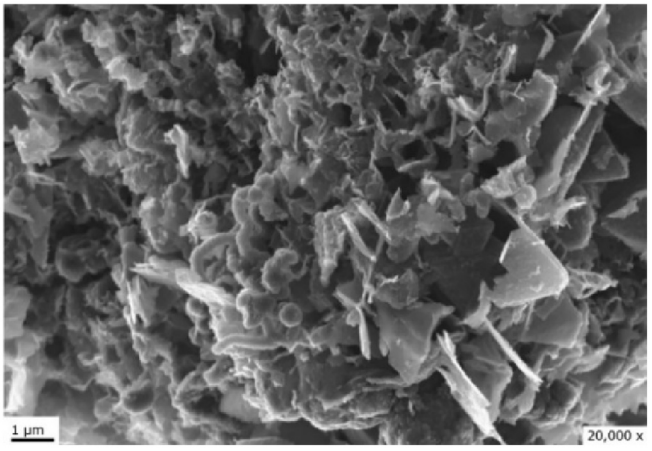

Fig. 3. SEM image taken at 20,000× magnification of carbon deposited in the manner previously described.

1350 cm^{-1} indicating that the synthesised carbons do not contain any sizeable quantity of functionalised hydrogen or hydroxyl groups [41]. There was, however slightly decreased transmittance in the region of 1650–1500 cm^{-1}, which is indicative of the presence of functionalised oxygen and of sp^3 hybridised carbon [41]. Abundant C-C bonds were observed from 1100 to 750 cm^{-1} in all samples [41]. The overall structure of the synthesised carbon was therefore concluded to be a combination of sp^2 and sp^3 hybridised carbon with some functionalised oxygen groups likely being present at the carbon surface.

XPS was used to examine the chemical structure of synthesised carbons in greater detail. Low and high resolution spectra were taken for synthesised carbon in the O 1s and the C 1s region. Based on the results of FTIR analysis, synthesised carbons consist of sp^2 and sp^3 hybridised carbon and carbon bonded to oxygen. As such the C 1s peak in the examined carbons was attributed to the presence of carbon in C-C, C-O-, C═O, COO, CO_3 and C═C chemical environments. Using the general binding energies of carbons in these environments [42,43] curve fitting was carried out in the CasaXPS software to estimate the compositions of synthesised carbon (Table 1). Based on the data in Table 1 the synthesised carbon consists mostly of sp^3 hybridised carbon in a C-C bonding environment. There is, however, a considerable amount of both oxidised and sp^2 hybridised, C═C bonded carbon present in the synthesised material. Based on this it is likely that the synthesised carbons will be suitable both for the formation of an electric double layer with an appropriate electrolyte, and for faradaic reaction at functionalised sites bonded to oxygen. This will allow carbons produced in the manner described here to act as hybrid capacitors, with both EDLC and pseudocapacitive performance being present in the material. The relative magnitude of these capacitive contributions will be quantified during our SPECS-based study of the synthesised carbons.

The specific surface areas of the synthesised carbons were measured by taking 9-point adsorption isotherms. Typical isotherms for these carbons showed largely Type I structure [44], which is characteristic of porous solids with relatively small external surfaces [44], such as activated carbons or zeolites. The average BET SSA of the synthesised carbons was 560 $m^2 g^{-1}$. This is comparable to the surface areas for carbons produced in a similar manner by previous groups [19], but is considerably lower than the BET SSA of activated carbons [22,34].

3.3. Cyclic voltammetry

Typical CVs and anodic capacitances with cycle number for the synthesised carbon and activated carbon prepared through the pyrolysis of coconut husks are shown in Fig. 4. Voltammograms produced for both activated carbon and the electrodeposited carbons generated in this work showed a box like cyclic voltammogram typical of an EDLC; however, in all cases some slope was apparent during the cathodic and anodic sweep, indicating small resistances. In some cases divergence from the expected rectangular voltammetric shape was observed, which indicates the occurrence of pseudo-capacitive reactions; however, this divergence was not always present. This may be attributed in part to the relatively fast scan rate of 25 mV s^{-1} lowering the contribution of

Table 1
Estimated composition of synthesised carbon as calculated based on low and high resolution XPS.

Bonding Interaction	O 1s	C 1s	C-C	C-O-	C=O	COO	C=C
Relative Percent (%)	7.6	92.4	63.1	11.3	7.5	7.3	10.8

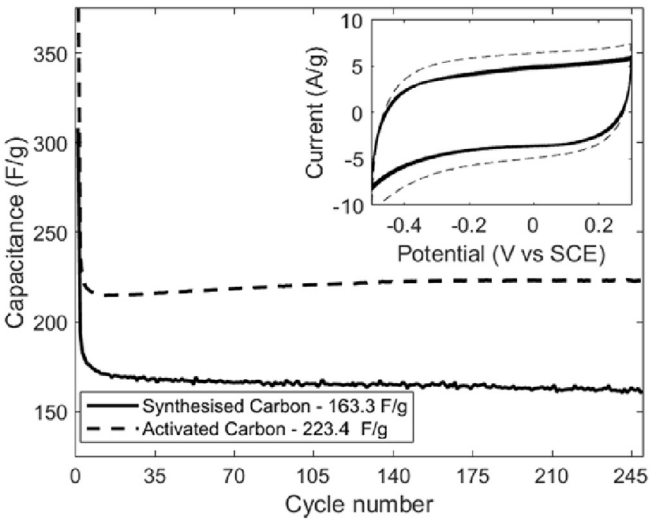

Fig. 4. The anodic capacitance of synthesised and activated carbon with cycle number and (inset) a CV of a synthesised carbon and an activated carbon taken in 0.50 M H_2SO_4. The scan rate was 25 mV s^{-1}.

diffusion processes to the capacitance of the examined materials, and, more notably, due to pseudo-capacitance in the examined materials likely arising from processes which occur across a wide potential range such as adsorption processes, which have been shown to cause little divergence from box-like cyclic voltammograms in manganese and ruthenium oxides [45]. The processes giving rise to pseudo-capacitance in the examined materials are further addressed in later sections of this report. The anodic capacitance of carbons were calculated by integrating the anodic current (i_A; A.g^{-1}) with respect to time (t; s) to give the anodic charge passed through the electrode over the time period under examination (Q; C.g^{-1}) for both the cathodic and anodic scans, which was related to the specific capacitance of the carbons by Refs. [35,36];

$$C = \frac{Q}{V} \tag{2}$$

where V is the potential window under examination (V). The specific capacitance relative to the cycle number is shown in Fig. 4(b). As shown, for both synthesised and activated carbons, both the cathodic and anodic capacitance changes considerably during initial cycles. This is consistent with the occurrence of irreversible anodic reactions on the carbon surface upon initial cycling. Such irreversible losses during the initial cycles have previously been observed to occur for activated carbons under identical conditions [35]. The total capacitance of synthesised carbons was consistently close to 160–180 F g^{-1}. This value compares favourably to the performance of commercially available activated carbon, which has previously been reported to have a capacitance between 118 and 130 F g^{-1} [35,36]; and also to the performance of carbon nanotube-derived supercapacitors (115 F g^{-1}) [12] and carbide-derived supercapacitive carbons (120–175 F g^{-1}) [20,46]. However, the performance of both the examined activated carbon (220 F g^{-1}) and, based on the results presented by previous groups [36], $RuO_2.nH_2O$ under these conditions (~400 F g^{-1}) is considerably higher than that of the synthesised carbon, as is that of hollow carbon nanospheres, which have been reported to show specific capacitances of 220–250 F g^{-1} in aqueous media [47,48]. The advantage that the electrodeposited carbons have over these materials is in the simplicity, cheap precursors and, compared to

nanotube synthesis particularly, low energy input of the carbon synthesis method. In addition to this, carbon synthesis through molten carbonate reduction has been highlighted by previous groups as a potential method of converting waste carbon dioxide from industry into value-added carbon products [19], which is itself a major area of interest for further research. As such carbon synthesis through molten carbonate reduction was judged to be a viable and interesting method of carbon synthesis which merits further investigation.

3.4. Step potential electrochemical spectroscopy analysis

Step potential electrochemical spectroscopy (SPECS) was used to examine the electrochemical performance of the electrodeposited carbons.

3.4.1. Modelling SPECS results

SPECS experiments were carried out as detailed in the methodology. Following collection of SPECS data the current response profiles for each examined carbon were analysed. A typical current response across the entirety of a SPECS experiment is shown in Fig. 5. As seen in Fig. 5 each potential step causes a spike in the current passing through the tested electrode. This current rapidly decays to a baseline value. The manner in which this current decay occurs provides us with a great deal of information on the processes occurring close to or at the electrode-electrolyte interface.

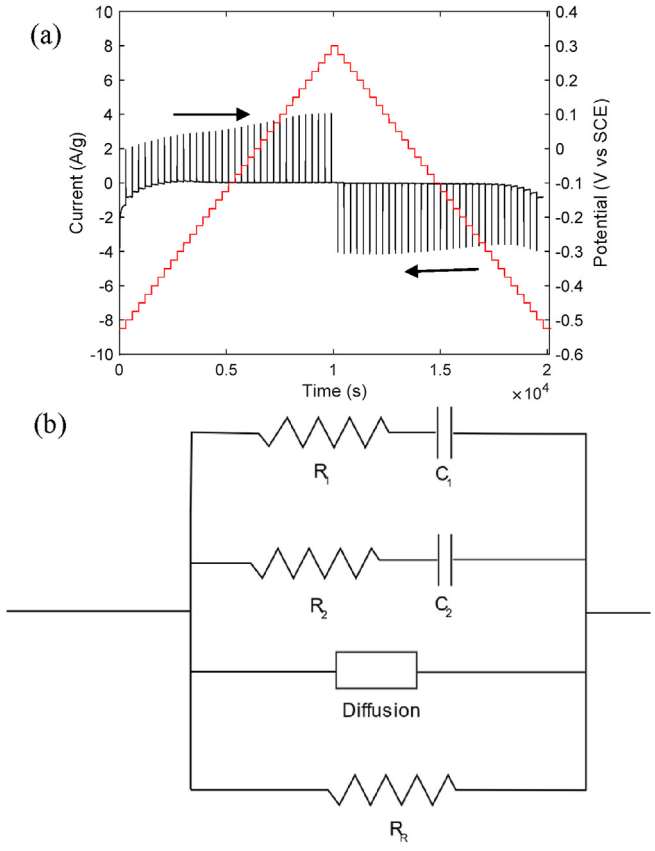

Fig. 5. (a) Current vs. time and potential during the step potential electrochemical spectroscopy (SPECS) analysis of electrochemically generated carbon in 0.5 M H_2SO_4 electrolyte. The red line represents the potential (right hand axis) and (b) the equivalent circuit for the examined cell based on the modelled processes. (For interpretation of the references to colour in this figure legend, the reader is referred to the Web version of this article.)

The current response for a EDLC in series with a resistor following a potential step of magnitude E (V) is given by Ref. [49]:

$$i_C = \frac{\Delta E}{R_S}\exp\left(-\frac{t}{R_S C_{DL}}\right) \quad (3)$$

where R_S ($\Omega \cdot g$) is the series resistance, C_{DL} is the double layer capacitance of the active material ($F.g^{-1}$), ΔE is the change in potential (V) over the duration of the potential step, and t is the time (s) during each individual potential step. In porous materials, such as high surface area carbons, it has previously been demonstrated that the double layer current response for the material is most accurately described as the combination of two separate double layer capacitance terms, arbitrarily denoted C_{DL1} and C_{DL2} [50]. These terms correspond to the formation of a double layer in micro- and mesopores where ion transport is hindered due to longer pathways through pores and electric double layers overlapping, and to formation of a double layer on the external surface and in larger macropores where ion transport is not significantly hindered. Both C_{DL1} and C_{DL2} have an associated series resistance, denoted R_{S1} and R_{S2}. As such the current response of a porous EDLC upon the application of a potential step may be described by a combination of two current responses (i_{C1} and i_{C2}) which describe the current response associated with the formation of a double layer on the bulk surface and easily accessed macropores, and in the smaller micro- and meso-pores, respectively.

In addition to double layer capacitances, carbonaceous materials are capable of exhibiting pseudo-capacitance, which may be attributed to the reversible redox reaction of functional groups at or close to the surface of the materials with electrolyte species. The presence of functional groups near the surface of the synthesised carbons have been highlighted previously in this research through both FTIR and XPS studies. Based on this it may be assumed that the carbon examined here exhibit some pseudo-capacitive behaviour. Pseudo-capacitive behaviour comes about due to the diffusion of reactive species at or near the surface of the active material, as such part of the current response observed during SPECS is given by the current response to diffusion of active species towards or away from the carbon surface. This contribution is denoted i_D ($A.g^{-1}$) and it may be modelled using the Cottrell equation for semi-infinite planar diffusion, [35,51]; i.e.,

$$i_D = nFA\Delta C\left(\frac{D}{\pi t}\right)^{1/2} = \frac{A_1}{t^{1/2}} \quad (4)$$

where i_D is diffusional current density ($A.g^{-1}$), n is the number of electrons involved in the redox process, F is Faraday's constant ($96486.7C\,mol^{-1}$), A is the electrochemically active surface area ($m^2.g^{-1}$), D is the diffusion coefficient for the redox system ($m^2.s^{-1}$), ΔC is the change in the ion concentration in the electrode structure over the duration of the time step ($mol.m^{-3}$), A_1 is an equivalent term assumed to be constant at a given potential, and t is the time (s).

It should be noted that, following a potential step, the current in Fig. 5 does not always decay to zero, often equilibrating at a small non-zero current. This current likely originates from slow, constant redox reactions between the active material and the electrolyte, leading to the occurrence of a residual current (i_R) that does not disappear between potential steps. Based on this, the total current response of many materials which show a hybrid-type capacitive performance (i_T) may be modelled by Ref. [36]:

$$i_T = i_{C1} + i_{C2} + i_D + i_R = \frac{\Delta E}{R_{S1}}\exp\left(-\frac{t}{R_{S1}C_{DL1}}\right) + \frac{\Delta E}{R_{S2}}\exp\left(-\frac{t}{R_{S2}C_{DL2}}\right) + \frac{A_1}{t^{1/2}} + A_2 \quad (5)$$

Based on these contributions the equivalent circuit cell shown in Fig. 5(b) was derived. The diffusion term refers to a combination of capacitor-like and resistor-like elements which decays relative to $t^{1/2}$, R_R refers to the resistance to the residual current, which is present throughout potential steps. R_1, C_1, R_2 and C_2 refer to the resistances and capacitances associated with electric double layer formation. The total current passing through the cell is a combination of the current passing through these various double layer, pseudocapacitive and residual processes. Eqn (5) was used in combination with least squared error regression methods to obtain fitted curves and estimates for the values of R_{S1}, C_{DL1}, R_{S2}, C_{DL2}, A_1 and A_2 at each potential step. The accuracy of the fit for each least squared error regression was judged by plotting the percent deviation between each estimated curve and the experimental data. This percent deviation was low, being at its highest when the current response was at its largest. At this point the percent deviation was generally less than ±2% of the total current. Due to the low magnitude of this deviation it was concluded that the parameters extracted from the model will be a good estimate as to the behaviour of the system.

3.4.2. EDLC and pseudo-capacitive contributions

The total capacitive behaviour of the examined carbons, as previously indicated, can be separated into contributions from the parts of the material that act as an ELDC and as a pseudocapacitor. This is achieved by separating the various parameters (R_{S1}, R_{S2}, C_{DL1}, C_{DL2}) which relate to the EDLC type behaviour of the material from the pseudo-capacitive parameter (A_1) and the residual parameter (A_2). By examining the manner in which these parameters vary with potential we can gain a great deal of information about the system under examination.

3.4.2.1. The series resistance. The series resistance of a cell is a major contributing factor to the overall power output (P, Wh.kg^{-1}), with lower series resistances correspond to increased power

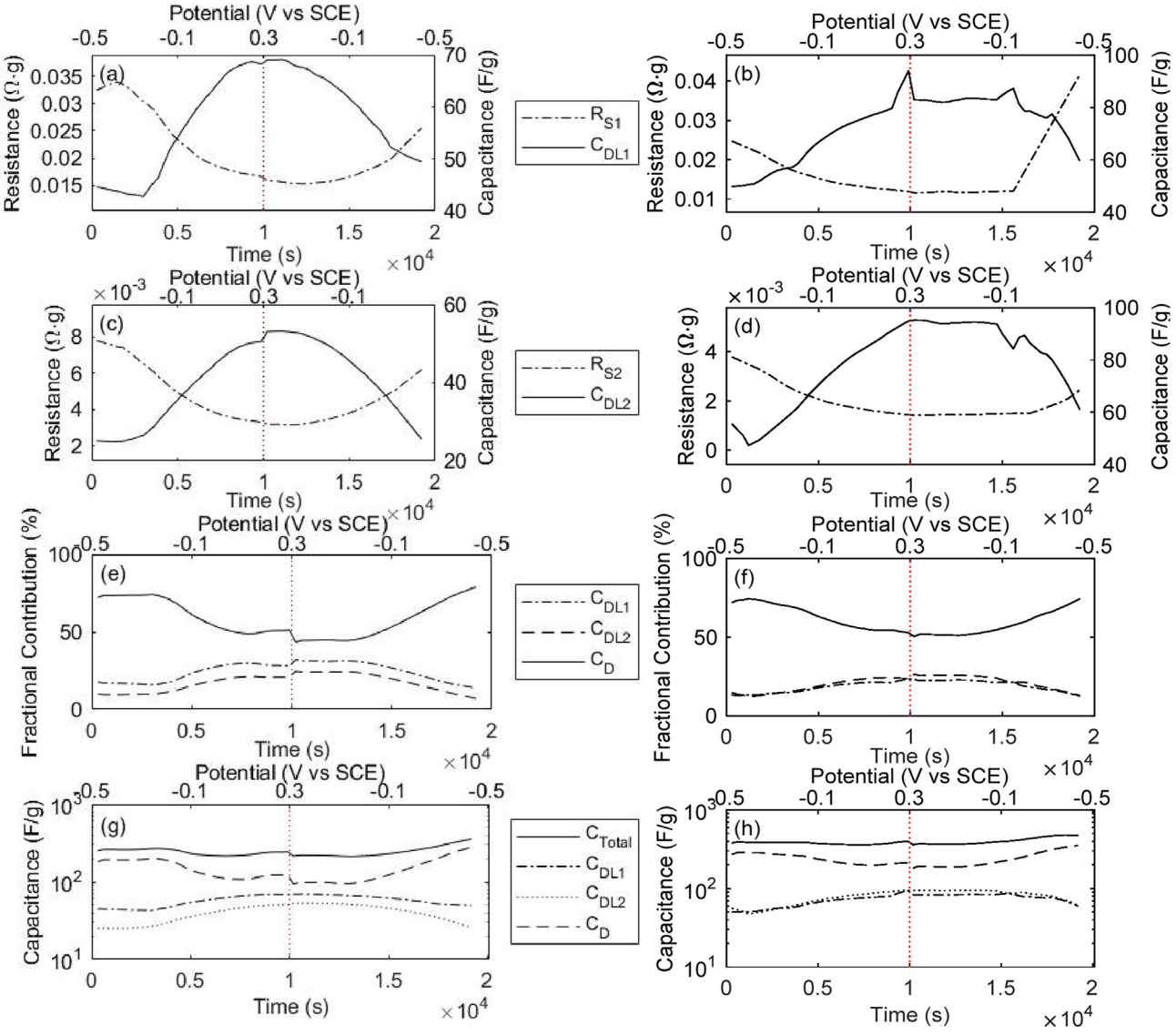

Fig. 6. (a)–(b) R_{S1} and C_{DL1} with potential (V vs SCE) and time (s) for synthesised carbon and activated carbon respectively, (c)–(d) R_{S2} and C_{DL2} with potential and time for synthesised and activated carbon respectively, (e)–(f) percentage contribution to the total capacitance of synthesised carbon and activated carbon respectively, and (g)–(h) total C_{DL1}, C_{DL2}, and C_D for synthesised carbon and activated carbon respectively.

outputs. In the case of this system, there are two series resistances to consider, R_{S1} and R_{S2}, which correspond to the series resistance associated with the porous surface area of the carbon (R_{S1}), and the geometric surface area of the carbon (R_{S2}). The changes in series resistance values for the anodic and cathodic scans of both synthesised carbon and activated carbon prepared by previous groups through the pyrolysis of coconut husks [36] are shown in Fig. 6(a)-(d).

From Fig. 6(a) it can be seen that, for synthesised carbon, at potentials close to −0.5 V vs SCE during both the cathodic and anodic scans, R_{S1} exhibits its largest value of close to 0.03 Ωg. As the potential is swept anodically, R_{S1} decreases, dropping to below 0.02 Ωg at 0.3 V vs SCE. It can be seen from Fig. 6(b) that the R_{S1} values of activated carbon are lower than those of the synthesised carbon. As the system should be otherwise identical this indicates that resistance to double layer formation in the pores of activated carbon is lower than in the synthesised carbon. In both cases the variation observed in R_{S1} with potential can be explained partially by comparing Fig. 6 to the SPECS results across the entire potential window (Fig. 5). Upon doing this it becomes apparent that the largest values of R_{S1} correspond to peaks in the SPECS data set where significant residual currents (i_R) are apparent and where the baseline current does not decay to zero across the relaxation period. This increase is likely due to redox reactions occurring between the electrolyte and the carbon which increase the overall electrolyte or, more likely, electrode resistance, thereby increasing R_{S1}.

It was previously suggested that these residual currents may be due to slow redox reactions occurring between the electrolyte and the carbon material. Based on Fig. 6, the value of R_{S1} increases significantly at cathodic potentials below −0.2 V vs SCE. This is close to the expected reduction potential of hydrogen in 0.5 M H_2SO_4 (−0.241 V vs SCE) [35], hence it is likely that the residual current is due to hydrogen ad-atom formation [52]; i.e.,

$$H^+ + e^- \rightarrow H_{ad} \quad (6)$$

This hydrogen ad-atom formation could pose an issue in supercapacitor devices constructed using the carbon material as it could lead to the formation of hydrogen gas by way of:

$$2H_{ad} \rightarrow H_2 \quad (7)$$

$$H^+ + H_{ad} + e^- \rightarrow H_2 \quad (8)$$

which is not desired in a sealed/closed system. However, based on CV results presented previously, the tested cell shows good cycle stability, which indicates that any adsorbed hydrogen formed during the cathodic sweep is effectively re-oxidised during the anodic sweep. The formation of hydrogen ad-atoms on the carbon surface at cathodic potentials below −0.2 V vs SCE appears to lead to increased resistance in the electrode, explaining the increase in R_{S1} when approaching −0.2 V vs SCE from higher potentials. Overall the values of R_{S1} are low across the potential range examined, being in the range of 0.02–0.03 Ωg. The lowest values of R_{S1} are found at anodic potentials more positive than −0.2 V vs SCE, suggesting that carbon performance may increase further at more positive potential windows.

The behaviour of R_{S2} in both the synthesised and the activated carbon closely mimics that of R_{S1}, albeit on a considerably lower scale. Fig. 6(c) shows that R_{S2} also has a maximum value at cathodic potentials, with series resistances of up to 0.008 Ωg being obtained. The value of R_{S2} gradually decreases when heading towards anodic potentials, dropping to almost 0.003 Ωg at potentials close to 0.3 V vs SCE. This indicates that R_{S2} is also affected by the formation of hydrogen ad-atoms or other side-reactions in a similar manner to R_{S1}. Fig. 6(d) shows that the value of R_{S2} for activated carbon is almost half that of the synthesised carbon, so the resistance to electric double layer formation at the geometric surface area of activated carbon is lower than the equivalent resistance for synthesised carbons. The low relative magnitude of R_{S2} as compared to R_{S1} can be explained since, over the duration of a single potential step, access of the electrolyte to, and interaction of the electrolyte with, the surface within micro- and mesopores is greatly hindered compared to access to the geometric surface area of carbons, so we expect both the magnitude of R_{S1} and the size of changes in R_{S1} to be considerably greater than that of R_{S2}.

3.4.2.2. The double layer capacitance. A double layer capacitor does not undergo chemical changes upon charging and discharging, and as such, if the majority of a capacitors performance is due to EDLC effects the material should show good cycle stability. A high double-layer capacitance across a large potential range is a desirable property of a supercapacitor. Changes in the values of C_{DL1} and C_{DL2} were therefore examined based on the potential at which they were calculated for the entire SPECS duration for both synthesised and activated carbon (Fig. 6(a)-(h)).

Based on Fig. 6(a) and (c) and on Fig. 6(b) and (d) respectively, The values of C_{DL1} and C_{DL2} for both synthesised and activated carbon change in a manner inverse to those of R_{S1} and R_{S2}, with both C_{DL} values being at their lowest at cathodic potentials, and elevated at anodic potentials greater than −0.2 V vs SCE. For synthesised carbon, at cathodic potentials close to −0.5 V vs SCE C_{DL1} is ~48 F g^{-1}, however, as the potential is swept anodically, C_{DL1} increases markedly to a maximum of ~68 F g^{-1}. The behaviour of C_{DL2} mimics that of C_{DL1}, with low values being observed at cathodic potentials and higher values at anodic potentials; however, the magnitude of C_{DL2} is less than that of C_{DL1} across the potential range investigated. In general, C_{DL2} has minimum values of 25 F g^{-1} close to −0.5 V vs SCE, which increases to ~50 F g^{-1} close to 0.3 V vs SCE. The capacitance attributed to the external surface area of the synthesised carbons is between 50 and 75% of the capacitance due to the micro- and mesoporous surface area of the carbons. The difference between C_{DL1} and C_{DL2} is expected since, while the formation of an electric double layer in micro- and mesopores is hindered due to both the difficulty in electrolytes accessing the porous structure, and due to the overlapping of electric double layers in small pores [53], the examined carbons have a large porous surface area in which double layer formation can occur. The values of C_{DL1} and C_{DL2} for synthesised carbons are lower than the corresponding capacitances of activated carbon (Fig. 6(b), (d), (h)), with C_{DL1} and C_{DL2} for activated carbon reaching ~80 F g^{-1} and ~90 F g^{-1} respectively. C_{DL1} has a lower maximum value than C_{DL2} in this case. This is likely due to chemical activation using concentrated H_3PO_4 at high temperatures increasing the mesoporous character of the produced carbon [54], which contributes to the increased value of C_{DL1}.

The values of both double layer capacitance terms correspond to the highest double layer capacitances being obtained at potentials where the respective series resistance is at its lowest. This is reasonable as decreased series resistance may be due to decreased resistance to double layer formation, so anodic potentials are beneficial for both the reduction of the series resistance in the examined carbons, and for the increased EDLC-type behaviour of the examined carbons. As the residual currents are at their highest at cathodic than −0.2 V vs SCE, this indicates that a potential window starting from a value more positive than −0.2 V vs SCE may be optimal for the electrochemical performance of the examined carbon as double layer capacitors. Further testing would be necessary to determine how far beyond 0.3 V vs SCE this optimal

potential window expands. The average double layer capacitance for synthesised carbon across the entire SPECS duration, considering every sample, was found to be close to 98 F g^{-1}, which corresponded to less than half of the total capacitance excluding residual capacitance. This indicates that the diffusional contribution to the capacitive performance of the examined carbon was quite considerable. The large relative magnitude of C_D compared to C_{DL1} and C_{DL2} can be seen for synthesised carbon and activated carbon in Fig. 6(e) and (f) respectively.

3.4.2.3. Diffusional contributions. The carbons examined in this study showed behaviour characteristic of hybrid EDLCs and pseudocapacitors. To quantify the fraction of the capacitance arising from pseudocapacitive behaviour, the current due to diffusion of electrolyte ions to the surface (where they react with functional groups, resulting in pseudocapacitive behaviour) was calculated for both synthesised and activated carbons. This was used to calculate the capacitance due to diffusion for synthesised and activated carbons respectively (Fig. 6(g)-(h)).

Based on Fig. 6(g)-(h) we can see that C_D is considerably larger than C_{DL1} and C_{DL2}, with synthesised carbons showing C_D as large as ~200 F g^{-1} and activated carbon showing C_D of up to ~300 F g^{-1}. In all cases the changes in C_D with potential mirror the changes in C_{DL}, with, in the case of synthesised carbons, elevated C_D of ~200 F g^{-1} being observed at cathodic potentials, and reduced C_D of ~100 F g^{-1} being observed at more positive potentials. These changes in C_D with potential are likely due to the nature of the functionalisation of the examined carbons, which we believe to be largely oxygen functionalisation. As we approach more cathodic potentials from 0 V vs SCE we approach the reduction potentials of the oxygen groups in carbonyl, then in carboxyl environments [55]. Based on this, depending on the degree of functionalisation of a material, as the cathodic limit is approached, we expect a greater number of functional sites to be reduced and an elevated C_D to be apparent.

3.4.2.4. The total capacitance (C_T). The total capacitance of the examined carbon electrodes takes into account the contributions from C_{DL1}, C_{DL2}, and C_D. The average value of C_T across all synthesised carbons at a scan rate of 0.5 mV s^{-1} was found to be ~275 F g^{-1}, Since the changes in the values of C_{DL1} and C_{DL2} are mirrored by the changes in C_D with potential, the value of C_T is mostly stable across the −0.5 to 0.3 V vs SCE potential window. The C_T value for synthesised carbon is considerably higher than those reported for commercially available activated carbons and carbon nanotube supercapacitors [9–11], and is more than 90 F g^{-1} higher than the capacitance of these carbons as calculated using cyclic voltammetry (Fig. 4). While some of this difference may be attributed to variation in the capacitance of materials as calculated using different techniques [56,57], the variation is largely due to the relative scan rates used for the two techniques, with cyclic voltammetry taking place at a scan rate of 25 mV s^{-1} and SPECS at 0.5 mV s^{-1}. The much slower scan rate of SPECS allows for greater electrolyte diffusion into pores and increased diffusional contributions, so an elevated capacitance is expected, up to a degree dictated by the material in question, when examining the electrochemical performance of a material at a reduced scan rate. The C_T value of the tested activated carbon was ~400 F g^{-1}, which is higher than both the synthesised carbon and commercially available activated carbons.

3.4.2.5. Scan rate studies. While it may seem at first that the techniques used to calculate capacitances during SPECS and CV experiments are completely different, there are actually considerable similarities between SPECS and CV. Most potentiostats carry out cyclic voltammetry not through the application of a continuously increasing potential, but through the application of a series of very small potential steps with a short rest period between [35]. Most equipment then measures the current over each potential step, by default, through averaging the current over the entire duration of the potential step and recording the average current as the current at the potential after the step. By this definition the major difference between a SPECS experiment with a potential step of ±25 mV measured over 50 s, and a CV experiment with a scan rate of 0.5 mV s^{-1}, is that during the cyclic voltammetry experiment the currents are averaged over a much smaller potential step. During SPECS the potential sweep rate (v, mV.s^{-1}) can be related back to the size of the time step being examined (t; s) and the size of the potential step (ΔE; V) through:

$$v = \frac{\Delta E}{t} \tag{9}$$

By examining a smaller or larger section of the experimental current-time curve, we can effectively control the sweep rate at which the SPECS experiment model proceeds. Doing this does, however, ignore entire segments of the SPECS results, hence it assumes that the ignored segments of the SPECS dataset do not hold any influence over the current change during subsequent potential steps. This is justified through noting that individual peaks during SPECS relax to a stable baseline value, the residual current, over the course of the 300 s relaxation period, so there should be no major effects from previous excitations on the current during subsequent steps. Based on this, equivalent cyclic voltammograms may be constructed for a range of scan rates from the averaged current at each potential step. Across all scan rates, these voltammograms show a general box-like voltammogram shape. Box-like voltammograms are characteristic of capacitive materials, so are generally expected when examining these materials. Additionally the magnitude of the observed current at each potential increases with increased scan rate. The generation of cyclic voltammograms at a variety of scan rates allows for the determination of how the specific capacitances of the tested carbons vary with a change in scan rate, which is a factor of interest when determining if a material will be of use in a supercapacitor device. The capacitance of both synthesised and activated carbons at each scan rate was broken down into its double layer and diffusional contributions using the deconvoluted SPECS data (Fig. 7).

Based on Fig. 7(a)-(b) it is apparent that, as scan rate increases, the total capacitance of the synthesised and activated carbon decays. For synthesised carbons at high scan rates (125 mV s^{-1}) the value of C_{Total} is ~25 F g^{-1}. This indicates that, at scan rates such as this, both diffusional and double layer processes are severely kinetically limited, so the produced carbons are largely unsuitable for capacitor applications at these scan rates. At a scan rate of 25 mV s^{-1} C_T is usually ~100 F g^{-1}. This value is lower than that calculated using CV; however, this is expected as previous groups have already addressed differences between the capacitance calculated using CV and other techniques, particularly those involving linear modelling such as SPECS [56,57].

The value of C_D is heavily affected by scan rate, decreasing in a manner similar to exponential decay. At slow scan rates of 0.0833 mV s^{-1} C_D is ~375 F g^{-1}, whereas at fast scan rates of 125 F g^{-1} this value drops to close to 5 F g^{-1}. At these high scan rates the value of C_D is lower than that of C_{DL1} and C_{DL2}. This is expected as it has been indicated already that the diffusional processes are slower than double-layer formation, due largely to their dependence on ion diffusion prior to charge density transfer to form adsorbed species as opposed to the localised charge separation which gives rise to double layer capacitances, so at fast scan rates a

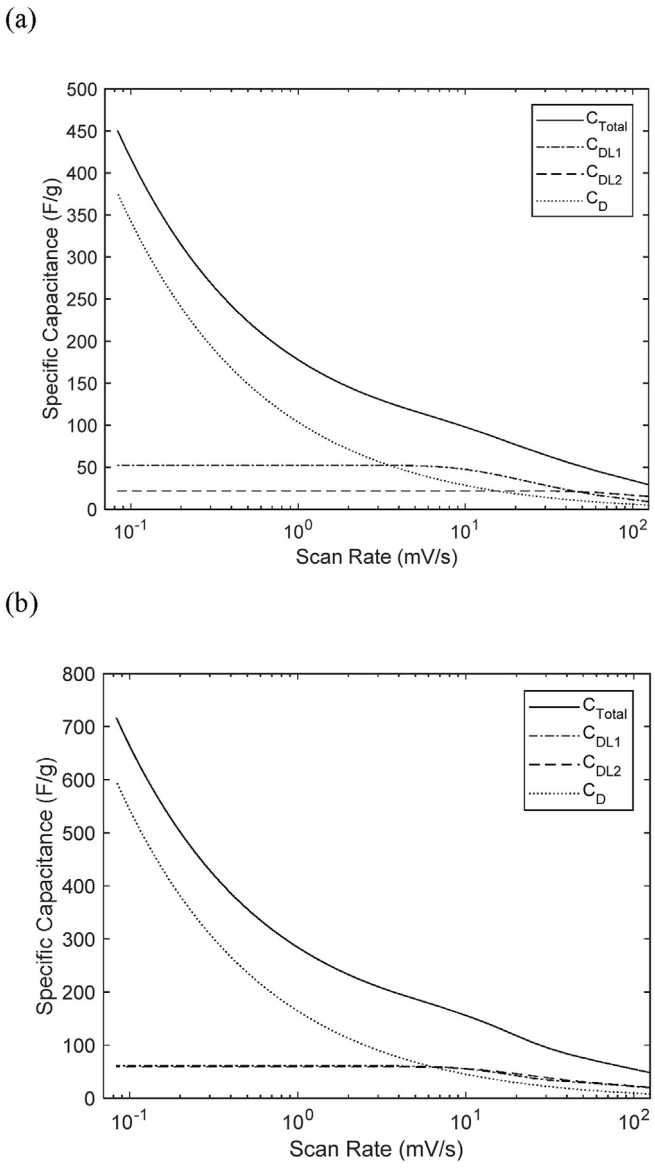

Fig. 7. (a) The specific capacitance of synthesised carbon (C_{Total}) plotted against individual double layer and diffusional contributions (C_{DL1}, C_{DL2}, C_D) and scan rate (b) the specific capacitance of an activated carbon with scan rate.

considerable decrease in C_D is observed but only a relatively slight decrease in C_{DL1} and C_{DL2}. Due to the presence of an acidic electrolyte, a combination of hydrogen or hydronium ion adsorption/desorption processes likely contribute to the total pseudocapacitance of the examined carbon materials by way of reactions similar to that shown in Eqn (10), the rate of adsorption itself is expected to be rapid, so the rate of these reaction are limited by the rate of ion diffusion from electrolyte into pores and onto the surface of the examined carbon materials.

$$C_{surface} + H_3O^+ + e^- \leftrightarrow CH_{ads} + H_2O \quad (10)$$

Reactions of this form have previously observed on MnO_2 supercapacitors and can contribute to adsorption pseudocapacitances which can be between 10 and 100 times greater than the potential double layer capacitance of an electrode [45,58].

At slow scan rates of 0.1 mV s^{-1} total capacitances of close to 450 F g^{-1} are obtained. This capacitance is unlikely to be the highest obtainable in the examined carbons as no plateau is observed in Fig. 7(a) at low scan rates The reason no low scan rate plateau is observed in Fig. 7(a) is because, even at the slowest scan rates, all active functional groups at the material surface have not been occupied by adsorbed ions. Particularly active sites within pores are expected to require extremely slow scan rates to become saturated. At slower scan rates than those examined here there should exist a point where groups are no longer being further occupied so a plateau shall appear. The contribution to the total capacitance of both C_{DL1} and C_{DL2} is more stable with scan rate, with C_{DL1} being stable at ~50 F g^{-1} up to 10 mV s^{-1} and C_{DL2} being stable at ~22 F g^{-1} up to scan rates of almost 50 mV s^{-1}, and only slightly decreasing past this point. This is as double layer formation is faster than faradaic processes, so both C_{DL} values are less affected by scan rate than C_D. C_{DL1} is more affected by scan rate than C_{DL2} as double layer formation in the pores of a material is dependent on sufficient time for electrolyte ions to access the pore structure of the material. This time is not reached at scan rates in excess of 10 mV s^{-1}, so a decrease in the capacitance, to the point where C_{DL1} is larger, is observed at scan rates in excess of this. For capacitive applications where a good double layer performance is desired a scan rate of anywhere for 0.0833 mV s^{-1} to 10 mV s^{-1} is suitable for these carbons. Fig. 7(b) indicates that the changes in the capacitance of activated carbon with scan rate mirror those of synthesised carbon, however the C_T value of activated carbon is higher than that of synthesised carbon, with capacitances as high as 700 F g^{-1} being obtained at slow scan rates. Overall the C_T of activated carbon at low scan rates tends to be ~1.5× that of the synthesised carbon examined here.

Based on the specific capacitance values presented in Fig. 7, it is possible to evaluate the specific energy and the specific power of the examined carbon system over a range of scan rates. It should be noted that the resultant Ragone diagrams are only fit for comparison to other materials tested under similar conditions as Ragone diagrams generally account for the total mass of an energy storage device rather than simply for the mass of the working electrode material [36]. In spite of this, a Ragone diagram allows for further comparison of the relative contributions of double layer and diffusion effects on the performance of the tested carbons. The specific energy and specific power of the tested carbons were calculated using [59,60]:

$$E = \frac{CV^2}{2} \quad (11)$$

$$P = \frac{E}{t} \quad (12)$$

where E is specific energy (Wh.kg^{-1}), P is specific power (W.kg^{-1}), V is the voltage window (V), C is the specific capacitance calculated with respect to scan rate (F.g^{-1}), and t is the time period used to produce the voltammogram for a specific scan rate (h). The calculated values for E and P were plotted, for the overall data set, as well as both double layer and diffusional processes to form Ragone diagrams such as those presented in Fig. 8(a)-(b).

Based on Fig. 8 it is apparent that, for both synthesised and activated carbon, as the scan rate increases, so too does the specific power of the examined carbons. Activated carbon shows a similar Ragone diagram to synthesised carbon, however the specific power of activated carbon at all scan rates is higher than that of the synthesised carbon. At low scan rates, diffusional contributions largely

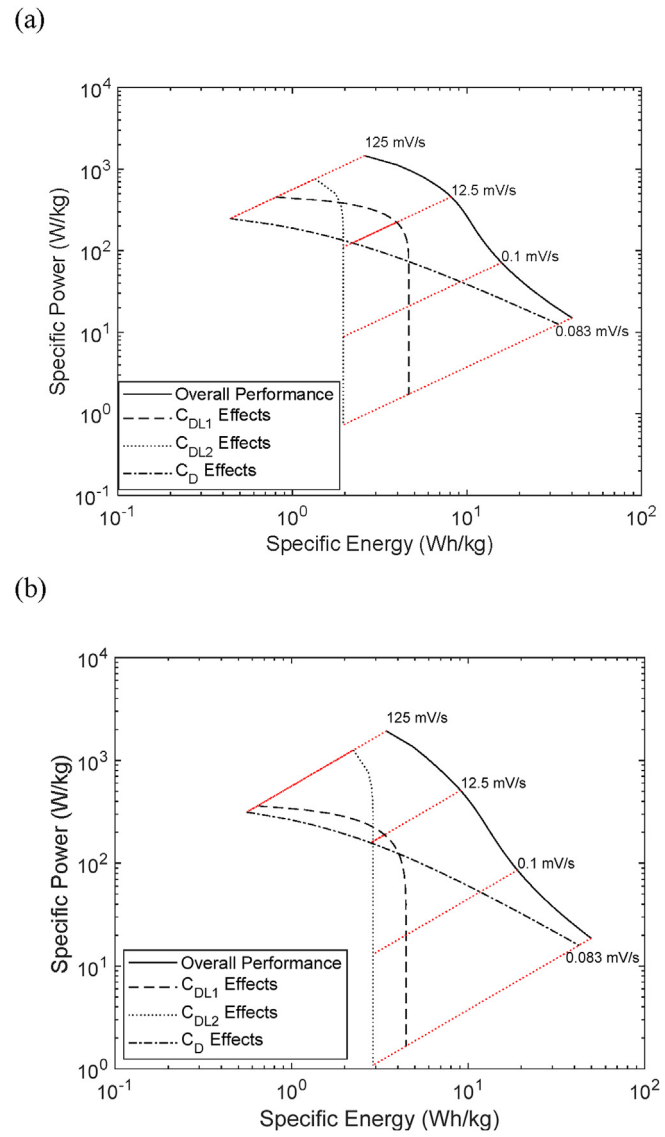

Fig. 8. (a) Ragone diagram for synthesised carbon based on the results of SPECS and (b) Ragone diagram for activated carbon based on the results of SPECS.

control the specific energy and power of the tested carbons, with both double layer effects contributing far less. At these low scan the contributions made by diffusion are larger than those contributed by double layer considerations. This makes sense as, at slow scan rates, diffusional contributions considerably outweigh double layer contributions to the capacitive performance of the examined carbons. These diffusional processes are kinetically limited at high scan rates, so as the scan rate increases we observe a decrease in diffusional contributions to the total electrochemical performance of the examined carbons as supercapacitor materials. This drop is not observed in the case of double layer contributions, which tend to show fairly constant specific energy and increasing specific power at increased scan rates scan rates in excess of 10 mV s^{-1}, whereupon, as expected based on the previous section, the specific energy due to C_{DL1} effects decreases significantly to lower than that due to C_{DL2} effects. Based on Fig. 8, and in agreement with previous results, the maximum pseudocapacitive performance of examined carbons can be obtained through cycling the carbon at very slow scan rates. At all examined scan rates the synthesised and activated carbons acted as hybrid capacitors with both EDLC and pseudocapacitive contributions contributing to the total electrochemical performance of the materials.

4. Conclusions

Carbons have been produced through the electrolytic reduction of molten lithium, sodium and potassium carbonates at the eutectic composition at 600 °C and 0.30 A cm^{-2}, under a CO_2 flow of 60 mL.min^{-1}. Carbon deposition occurs through the 4-electron reduction of carbonate ions. The resultant carbon consists of amorphous phases together with spherical and flake-like conglomerates. The BET SSAs of the deposited carbons were greater than 500 m^2 g^{-1} prior to any activation techniques being applied. Produced carbons were analysed through the use of cyclic voltammetry at a sweep rate of 25 mV s^{-1}, which revealed that the carbons showed good cycle stabilities in aqueous acid media across the first 250 cycles. Integration of the area under the anodic and cathodic sweeps of the cyclic voltammogram have shown that the specific capacitance of carbons produced in the manner described above change considerably over the first 10–50 scans, before stabilising to values close to 180 F g^{-1}. This is superior to the capacitive performance reported based on SPECS analysis at fast scan rates (130 F g^{-1}), however both reported values are either comparable or superior to the performance of commercially available activated carbons. As such carbon produced in this manner may constitute a superior material for supercapacitor applications.

SPECS has successfully been shown to be able to calculate electrochemical characteristics of carbons. It has been demonstrated that SPECS embodies an excellent method of separating and comparing the EDLC and pseudocapacitor-type performance of potential supercapacitor materials. Due to this SPECS shows several advantages over more conventional electrochemical testing techniques such as cyclic voltammetry and chronoamperometry, which only provide a relatively limited amount of information on the electrochemical characteristics of supercapacitor materials.

Synthesised carbon have been shown to have specific capacitances of close to 25 F g^{-1} at scan rates of 125 mV s^{-1}, and specific capacitances as high as 450 F g^{-1} at slow scan rates of 0.0833 mV s^{-1}. Both the double layer capacitance and the capacitance due to diffusion of synthesised carbons have been shown to be dependent on potential, with anodic potentials producing the highest double layer capacitances and lowest diffusional capacitances, and with cathodic potentials giving rise to relatively high capacitances due to diffusion and low double layer capacitances. The capacitance due to the porous area of synthesised carbons (C_{DL2}) has been shown to be 50–75% greater than the capacitance due to the geometric surface area (C_{DL1}) of the synthesised carbons at a scan rate of 0.5 mV s^{-1}, and the total double layer capacitance of synthesised carbons has been shown to be, on average, less than half of the capacitance due to diffusion in the synthesised carbons. As such, at slow scan rates, synthesised carbons act as hybrid capacitors with large pseudocapacitive contributions. This changes at high scan rates in excess of 5 mV s^{-1} when there is not sufficient time for diffusion limited processes to occur, so at high scan rates synthesised carbons act as hybrid capacitors with mainly EDLC contributions. This means that the cycle life and specific power of the synthesised carbons is increased at high sweep rates, however this is at the cost of decreased capacitive performance and decreased specific energy.

Synthesised carbon performed inferiorly to activated carbon produced through the pyrolysis of coconut husks, which showed capacitances as high as 700 F g^{-1} at low scan rates and which also showed considerable hybrid capacitor performance, however synthesised carbons performed superiorly to the reported performance of many commercially available activated carbons. As such it

will likely be beneficial to activate the synthesised carbon for increased supercapacitive performance. The residual currents present throughout SPECS were high at cathodic potential, particularly at potentials more cathodic than −0.2 V vs SCE. As such a more anodic potential window may reduce side-reactions in this system, with the trade-off of slightly reduced pseudocapacitive performance and increased EDLC-type performance.

Acknowledgements

MAH would like to acknowledge the University of Newcastle for the provision of a PhD Scholarship. The authors also acknowledge the support of the EMX Unit at the University of Newcastle.

References

[1] S. Chu, A. Majumdar, Nature 488 (2012) 294–303.
[2] M. Vangari, T. Pryor, L. Jiang, J. Energy Eng. 139 (2013) 72–79.
[3] V. Musolino, E. Tironi, in: Electrical Systems for Aircraft, Railway and Ship Propulsion (ESARS), IEEE, Bologna, 2010, pp. 1–6.
[4] R. Kötz, M. Carlen, Electrochim. Acta 45 (2000) 2483–2498.
[5] M.D. Stoller, S. Park, Y. Zhu, J. An, R.S. Ruoff, Nano Lett. 8 (2008) 3498–3502.
[6] M. Winter, R. Brodd, Chem. Rev. 104 (2004) 4245–4269.
[7] Q. Wang, L. Jiao, H. Du, Y. Wang, H. Yuan, J. Power Sources 245 (2014) 101–106.
[8] P. Jampani, A. Manivannan, P. Kumata, Electrochem. Soc. Interface (2010) 57–62. Fall 2010.
[9] F. Béguin, E. Frackowiak, Surface chemical and electrochemical properties of carbons, in: F. Béguin, E. Frackowiak (Eds.), Carbons for Electrochemical Energy Storage and Conversion Systems, CRC Press, Florida, 2010, p. 191.
[10] W. Gu, G. Yushin, WIREs Energy and Environ. 3 (2014) 424–473.
[11] P. Simon, A. Burke, Electrochem. Soc. Interface (2008) 38–43 spr08.
[12] J.H. Chen, W.Z. Li, D.Z. Wang, S.X. Yang, J.G. Wen, Z.F. Ren, Carbon 40 (2002) 1193–1197.
[13] R. Signorelli, D.C. Ku, J.G. Kassakian, J.E. Schindall, Proc. IEEE 97 (2009) 1837–1847.
[14] C. Masarapu, H.F. Zeng, K.H. Hung, B. Wei, ACS Nano 3 (2009) 2199–2206.
[15] L. Permann, M. Latt, J. Leis, M. Arulepp, Electrochim. Acta 51 (2006) 1274–1281.
[16] J.A. Fernández, S. Tennison, O. Kozynchenko, F. Rubiera, F. Stoeckli, T.A. Centeno, Carbon 47 (2009) 1598–1604.
[17] M. Lazzari, M. Mastragostino, A.G. Pandolfo, V. Ruizb, F. Soavi, J. Electrochem. Soc. 158 (2010) A22–A25.
[18] R. Crabtree, Supercapacitors: electrode materials aspects, in: R. Crabtree (Ed.), Energy Production and Storage: Inorganic Chemical Strategies for a Warming World, John Wiley and Sons Ltd., West Sussex, 2010, pp. 347–350.
[19] H. Yin, X. Mao, D. Tang, W. Xiao, L. Xing, H. Zhu, D. Wang, D.R. Sadoway, Energy Environ. Sci. 6 (2013) 1538–1545.
[20] J. Chmiola, G. Yushin, R.K. Dash, E.N. Hoffman, J.E. Fischer, M.W. Barsoum, Y. Gogotsi, Electrochem. Solid State Lett. 8 (2005) A357–A360.
[21] M.A. Hughes, J.A. Allen, S.W. Donne, Electrochim. Acta 176 (2015) 1511–1521.
[22] K. Le Van, H. Groult, F. Lantelme, M. Dubois, D. Avignant, A. Tressaud, S. Komaba, N. Kumagai, S. Sigrist, Electrochim. Acta 54 (2009) 4566–4573.
[23] F. Lantelme, B. Kaplan, H. Groult, D. Devilliers, J. Mol. Liq. 83 (1999) 255–269.
[24] H. Groult, B. Kaplan, F. Lantelme, S. Komaba, N. Kumagai, H. Yashiro, T. Nakajima, B. Simon, A. Barhoun, Solid State Ionics 177 (2006) 869–875.
[25] H. Kawamura, Y. Ito, J. Appl. Electrochem. 30 (2000) 571–574.
[26] L. Massot, P. Chamelot, F. Bouyer, P. Taxil, Electrochim. Acta 47 (2002) 1949–1957.
[27] C. Baker, W. Charnock, A. Mitchell, I. Warren, Carbon 8 (1970) 402–404.
[28] H.V. Ijije, R.C. Lawrence, G.Z. Chen, RSC Adv. 4 (2014) 35808–35817.
[29] H.V. Ijije, C. Sun, G.Z. Chen, Carbon 73 (2014) 163–174.
[30] A. Cormie, A. Cross, A.F. Hollenkamp, S.W. Donne, Electrchim. Acta 55 (2010) 7470–7478.
[31] M.F. Dupont, A.D. Cross, A. Morei, M. Drozd, A.F. Hollenkamp, S.W. Donne, J. Electrochem. Soc. 160 (2013) A1219–A1231.
[32] G.J. Browning, S.W. Donne, J. Appl. Electrochem. 35 (2005) 871–878.
[33] M.R. Bailey, S.W. Donne, J. Electrochem. Soc. 158 (2011) A802–A808.
[34] M.F. Dupont, S.W. Donne, J. Electrochem. Soc. 162 (2015) A5096–A5105.
[35] M.F. Dupont, S.W. Donne, Electrochim. Acta 167 (2015) 268–277.
[36] M.F. Dupont, S.W. Donne, J. Power Sources 326 (2016) 613–623.
[37] M. Murai, K. Takizawa, K. Soejima, H. Sotouchi, J. Electrochem. Soc. 143 (1996) 3456–3462.
[38] R.C. Lawrence, in: Chemistry and Environmental Engineering, University of Nottingham, Nottingham, 2013, p. 237.
[39] E. Karg, G.A.E. Karg, G.A. Ferron, O. Schmid, O. Schmid, in: Institute for Inhalation Biology, German Research Center German Research Center for Environmental Environmental Health, 2008, p. 2.
[40] H.O. Pierson, Natural graphite, graphite powders, particles and compounds, in: Handbook of Carbon, Graphite, Diamond and Fullerenes: Properties, Processing and Applications, Noyes Publications, Park Ridge, New Jersey, USA, 1993, p. 227.
[41] G.H. Jeffery, J. Basset, J. Mendham, R.C. Denney, Infrared spectrophotometry, in: G.H. Jeffery (Ed.), Vogel's Textbook of Quantitative Chemical Analysis, Longman Scientific & Technical, New York, 1989, pp. 741–757.
[42] B. Kaplan, H. Groult, A. Barhoun, F. Lantelme, T. Nakajima, V. Gupta, S. Komaba, K. Kumagai, J. Electrochem. Soc. 149 (2002) D72–D78.
[43] M. Sardela, X-ray photoelectron spectroscopy (XPS) and auger electron spectroscopy (AES), in: M. Sardela (Ed.), Practical Materials Characterisation, Springer Science, New York, 2014, pp. 102–103.
[44] K.S. Sing, D.H. Everett, R.A. Haul, L. Moscou, R.A. Pierotti, J. Rouquérol, T. Siemieniewska, Pure Appl. Chem. 57 (1985) 603–619.
[45] M. Toupin, T. Brousse, D. Bélanger, Chem. Mater. 16 (2004) 3184–3190.
[46] M. Arulepp, J. Leis, M. Lätt, F. Miller, K. Rumma, E. Lust, A.F. Burke, J. Power Sources 162 (2006) 1460–1466.
[47] B. You, J. Yang, Y. Sun, Q. Su, Chem. Commun. 47 (2011) 12364–12366.
[48] X. Xia, Y. Zhang, Z. Fan, D. Chao, Q. Xiong, J. Tu, H. Zhang, J. Fan Hong, Adv. Energy Mater. 5 (2014), 1401709.
[49] A.J. Bard, L.R. Faulkner, Nonfaradaic processes and the nature of the electrode-solution interface, in: Electrochemical Methods: Fundamentals and Applications, John Wiley & Sons, New York, 2001, p. 15.
[50] M.F. Dupont, S.W. Donne, Electrochim. Acta 191 (2016) 479–490.
[51] A.J. Bard, L.R. Faulkner, Basic potential step methods, in: Electrochemical Methods: Fundamentals and Applications, John Wiley & Sons, New York, 2001, pp. 162–163.
[52] M.E. Martins, C.F. Zinola, A.J. Arvia, J. Braz. Chem. Soc. 8 (1997) 363–370.
[53] C.-H. Hou, in: School of Civil and Environmental Engineering Georgia Institute of Technology Georgia, 2008, p. 183.
[54] J.B. Castro, P.R. Bonelli, E.G. Cerrella, A.L. Cukierman, Ind. Eng. Chem. Res. 39 (2000) 4166–4172.
[55] A. Bar-Even, A. Flamholz, E. Noor, R. Milo, Nat. Chem. Biol. 8 (2012) 509–517.
[56] Metrohm, in, Metrohm Autolab, 2014, pp. 1–5.
[57] D.K. Kampouris, X. Ji, E.P. Randviir, C.E. Banks, RSC Adv. 5 (2015) 12782–12791.
[58] B.E. Conway, V. Birss, J. Wojtowicz, J. Power Sources 66 (1997) 1–14.
[59] M. Yu, W. Wang, C. Li, T. Zhai, X. Lu, Y. Tong, NPG Asia Mater. 6 (2014) e129.
[60] W. Lu, J.-B. Baek, L. Dai, Supercapacitor technology and performance, in: W. Lu, J.-B. Baek, L. Dai (Eds.), Carbon Nanomaterials for Advanced Energy Systems, John Wiley & Sons, New Jersey, 2015, pp. 301–302.